## EDGE ARTICLE

Check for updates

# Tuning vibration-induced emission through macrocyclization and catenation†

Wei-Tao Xu,[a] Zhiyong Peng,[a] Peicong Wu,[b] Yefei Jiang,[a] Wei-Jian Li,[a] Xu-Qing Wang,[a] Jinquan Chen, [ID][b] Hai-Bo Yang [ID][ac] and Wei Wang [ID]*[a]

In order to investigate the effect of macrocyclization and catenation on the regulation of vibration-induced emission (VIE), the typical VIE luminogen 9,14-diphenyl-9,14-dihydrodibenzo[a, c]phenazine (DPAC) was introduced into the skeleton of a macrocycle and corresponding [2]catenane to evaluate their dynamic relaxation processes. As investigated in detail by femtosecond transient absorption (TA) spectra, the resultant VIE systems revealed precisely tunable emissions upon changing the solvent viscosity, highlighting the key effect of the formation of [2]catenane. Notably, the introduction of an additional pillar[5]arene macrocycle featuring unique planar chirality endows the resultant chiral VIE–active [2] catenane with attractive circularly polarized luminescence in different states. This work not only develops a new strategy for the design of new luminescent systems with tunable vibration induced emission, but also provides a promising platform for the construction of smart chiral luminescent materials for practical applications.

## Introduction

Smart organic materials with tunable and switchable luminescence have shown great potential for wide applications such as imaging,[1] sensors,[2] and optical displays.[3] Therefore, the development of novel luminogens which are sensitive to external stimuli, such as light,[4] solvent polarity,[5] solvent viscosity,[6] pH,[7] ambient temperature,[8] and pressure,[9] remains an attractive topic. Among the diverse luminogens, single-molecule fluorophores with multiple emissions have received continuous attention due to their basic research interest and potential high-tech applications.[10] In particular, a series of dihydrophenazine (DHP) derivatives with anomalously large Stokes shifts and multiple emissions, especially ones based on the core of 9,14-diphenyl-9,14-dihydrodibenzo[a, c]phenazine (DPAC), have been successfully developed by Tian, Chou, and other groups.[11] DPAC exhibits a V-shaped bent conformation in the ground state, and under light excitation, its lowest excited state can relax into a nearly planar structure through the vibration of the

phenazine unit, ultimately resulting in long wave emissions, and thus they termed this interesting phenomenon as 'vibration-induced emission (VIE)'.[11a,b] Previous studies have proven that the vibrational transition from the bending state of the lowest excited state to the planar state can be efficiently regulated by external stimuli such as temperature or solvent viscosity, leading to multiple emission behaviors.[11c] Attributed to such attractive features, so far DPAC-based materials have been widely used in ion probes,[12] thermometers,[13] biosensors,[14] white light emitting materials[15] and so on.

Notably, the design of novel emitters with tunable VIE behaviors is not trivial. In previous studies, more attention has been paid to the locking of the DPAC unit through the formation of either covalent or noncovalent macrocycles. Such a design strategy has been proven to be reliable, leading to the expected tunable multi-color emissions for practical uses.[12b,c,16] Notably, considering that macrocycles could serve as the key components for the construction of mechanically interlocked molecules (MIMs) such as rotaxanes and catenanes, the further construction of DPAC-based MIMs will be of great importance. On one hand, the formation of MIMs would serve as an efficient method for emission regulation attributed to the confined yet flexible environment of the mechanical bond, thus possibly adding a new dimension for VIE tunability.[17] Notably, in their inspiring studies, Goldup *et al.* and Qu *et al.* have already proven the great power of mechanical bonds in regulating the emission performances of luminogens.[18] On the other hand, the existence of other components within DPAC-based MIMs makes them promising platforms for integration with other functional groups, thus endowing them with interesting properties and

[a]*Shanghai Key Laboratory of Green Chemistry and Chemical Processes, State Key Laboratory of Petroleum Molecular and Process Engineering (SKLPMPE), School of Chemistry and Molecular Engineering, East China Normal University, 3663 N. Zhongshan Road, Shanghai 200062, China. E-mail: wwang@chem.ecnu.edu.cn*

[b]*State Key Laboratory of Precision Spectroscopy, School of Physics and Electronic Science, East China Normal University, Dongchuan Road 500, Shanghai 200241, China*

[c]*Shanghai Center of Brain-inspired Intelligent Materials and Devices, East China Normal University, Shanghai 200241, China*

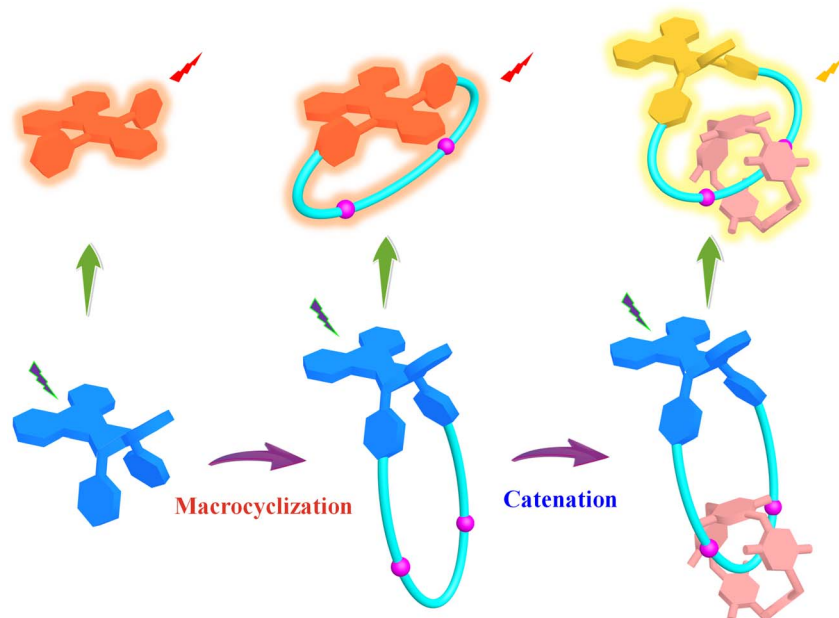† Electronic supplementary information (ESI) available. See DOI: https://doi.org/10.1039/d4sc00650j

**Fig. 1** Design strategy of the DPAC-functionalized macrocycle and chiral [2]catenane with tunable VIE behaviors.

functions. For instance, for DPAC-based [2]catenane with an additional chiral macrocycle, attractive circularly polarized luminescence (CPL) performances would emerge. However, the design and construction of novel DPAC-based MIMs, particularly chiral ones, have been rarely explored.

Based on our ongoing interest in MIMs,[19] particularly ones with switchable CPL,[20] in this study, the DPAC unit was inserted into the skeletons of a macrocycle and a corresponding [2]catenane with the pillar[5]arene macrocycle (Fig. 1). Detailed femtosecond transient absorption (TA) study suggested that the macrocyclization and catenation led to precisely tunable VIE behaviors upon changing the solvent viscosity. In addition, the introduction of pillar[5]arene with unique planar chirality[21] into the [2]catenane endows it with interesting CPL performances in different states, thus providing a new platform for the construction of smart chiral luminescent materials for practical applications.

## Results and discussion

### Design and synthesis of the DPAC-functionalized macrocycle and [2]catenane

In our design strategy, to investigate the influence of macrocyclization and catenation on the VIE behaviors, the DPAC unit as a typical VIE luminogen was first introduced into a macrocycle to tune the VIE through possible conformation locking. Moreover, an additional macrocycle was then combined with the resultant DPAC-functionalized macrocycle to give rise to the formation of corresponding DPAC-functionalized [2]catenane. More importantly, along with such a catenation process, enhanced conformation restriction would be achieved, possibly leading to interesting VIE behaviors. With such a design strategy in mind, in this study, in order to increase the synthetic efficiency, the [2]rotaxane **2** with diethyoxypillar[5]arene (DEP[5]

A) as the wheel component and pentafluorophenyl ester units as exchange stoppers as well as corresponding axle component **3** without DEP[5]A were first prepared (Scheme S1†).[22] Starting from key intermediate **1** with the DPAC core and two $NH_2$ tails, the targeted DPAC-functionalized [2]catenane **DPAC-C** and macrocycle **DPAC-M** were successfully synthesized through the transamidation reactions with **2** and **3**, respectively, in 27% and 32% yields under high dilute conditions(Fig. 2, Scheme S1†).

The resultant macrocycle **DPAC-M** and [2]catenane **DPAC-C** were well characterized by one-dimensional (1D) ($^1H$ and $^{13}C$) NMR and HRMS (ESI-TOF-MS) analysis. For instance, for macrocycle **DPAC-M**, the characteristic peaks at 5.60–5.57 ppm as typical signals for amide bonds were observed, which preliminarily proved the generation of the targeted macrocyclic structure (Fig. S14†). In the case of [2]catenane **DPAC-C**, the characteristic peaks attributed to both DPAC and DEP[5]A units with 1 : 1 integration ratio were observed, indicating the formation of an integrated molecule (Fig. S17†). Moreover, the proton signals attributed to the amide bonds ($H_5$) and methylene moieties ($H_{12}$) revealed remarkable upfield shifts due to the shielding effect of the DEP[5]A macrocycle, suggesting the formation of the expected interlocked structure (Fig. 3a). In addition, all the proton signals attributed to the DEP[5]A macrocycle displayed obvious upfield shifts, indicating that the **DPAC-M** ring in the [2]catenane structure also has a shielding effect on the DEP[5]A macrocycle. More importantly, in the HRMS (ESI-TOF-MS) spectra, single characteristic peaks ($m/z =$ 859.5127 and 1751.0162) attributed to $[\textbf{DPAC-M} + H]^+$ and $[\textbf{DPAC-C} + H]^+$ were observed, respectively, which are consistent with the theoretical values of 859.5162 and 1751.0165 (Fig. S16 and S19†), again confirming the successful synthesis of the targeted macrocycle and [2]catenane. Notably, in the $^1H$ NMR spectra of [2]catenane **DPAC-C** (Fig. 3a and S22†), only broadened signals with chemical shifts between −1.5 ppm and
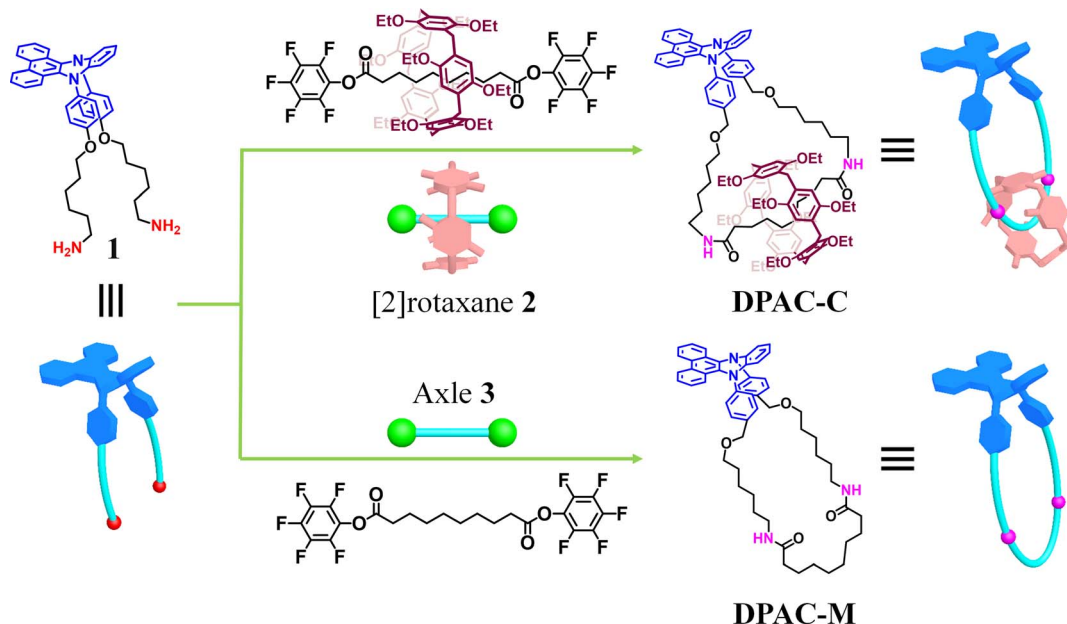
**Fig. 2** Synthesis of novel DPAC-functionalized macrocycle **DPAC-M** and [2]catenane **DPAC-C**. Reaction conditions: **1** (1.0 equiv.), **2** or **3** (1.0 equiv.), THF (~0.1 mM), r.t., 48 h, 27% for **DPAC-C** and 32% for **DPAC-M**.

2.5 ppm were observed, while the typical peaks of the pillararene/alkyl chain interlocked system were not found, which might be due to the rapid motion of the long alkyl chain moiety of the **DPAC-M** component. In order to further investigate such motion behavior of the **DPAC-M** component within the [2]catenane, ${}^1$H NMR spectra of [2]catenane **DPAC-C** at different temperatures were then collected. As shown in Fig. 3b and S23,† upon cooling the sample to −15 °C, broadened signals with chemical shifts in the range of −2.5 ppm to −1.0 ppm started to appear. Further lowering the temperature

to −75 °C led to the emergence of seven sets of signals in the range of −3.0 to 0.0 ppm, which can be attributed to the typical signals of the pillararene/alkyl chain interlocked system, again confirming the successful formation of the targeted [2]catenane skeleton. In addition, considering that the solvent viscosity would also influence the motion behaviors of the ring component, ethylene glycol (EG), which is highly viscous and miscible with THF, was then chosen to investigate the effect of solvent viscosity. Unfortunately, according to the ${}^1$H NMR study shown in Fig. S24,† the gradual increase in the proportions of EG-$d_6$ in
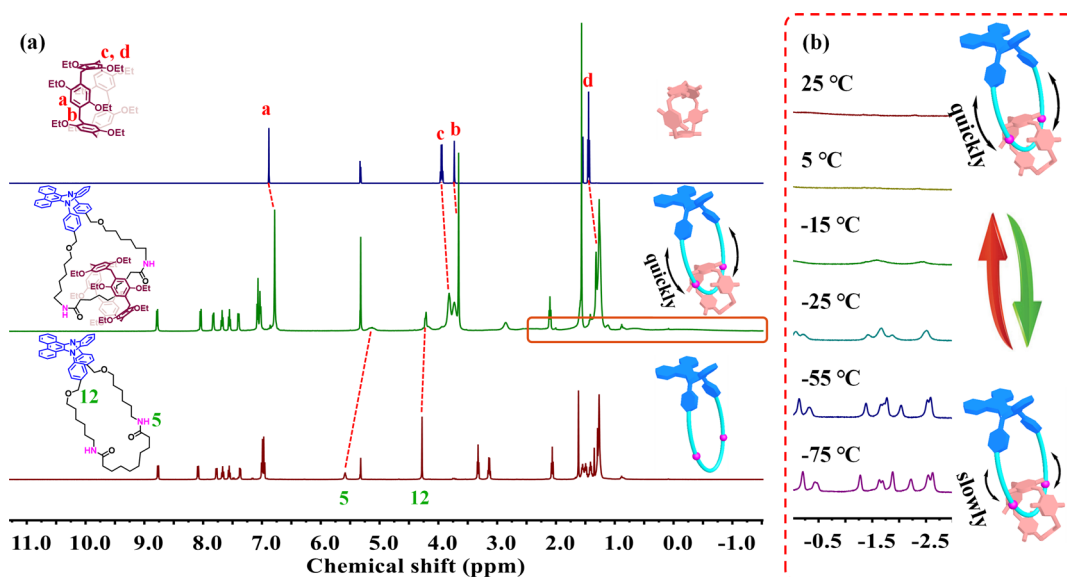


**Fig. 3** (a) ${}^1$H NMR spectra (CD$_2$Cl$_2$, 298 K, 500 MHz) of macrocycle **DPAC-M** (bottom), [2]catenane **DPAC-C** (middle), and the wheel component DEP[5]A (top); (b) partial ${}^1$H NMR spectra (CD$_2$Cl$_2$, 500 MHz) of [2]catenane **DPAC-C** at different temperatures. (Inset) cartoon representation of the motion behaviors of macrocycle **DPAC-M** within the [2]catenane **DPAC-C**.

THF-$d_8$ solution (0.5 mM) of [2]catenane **DPAC-C** did not lead to the emergence of the typical signals below 0 ppm, suggesting negligible effect of the solvent viscosity on ring component motions within the [2]catenane **DPAC-C**.

## Tunable VIE behaviors of the DPAC-functionalized macrocycle and [2]catenane

With the targeted DPAC-functionalized macrocycle **DPAC-M** and [2]catenane **DPAC-C** in hand, their steady-state photophysical properties were first measured in THF. As revealed by their normalized absorption and emission spectra shown in Fig. 4b, both the absorption onset and peak wavelength of macrocycle **DPAC-M** are similar to those of DPAC, both at 410 nm and 350 nm, respectively, indicating that the formation of the macrocycle does not remarkably change the absorption of DPAC in the ground state. Notably, the absorption peak of **DPAC-M** is slightly widened. However, for [2]catenane **DPAC-C**, obvious red shifts of both the absorption onset (to 415 nm) and peak wavelength (to 357 nm) were observed. These results suggested that along with the formation of [2]catenane **DPAC-C**, a more planar conformation of the DPAC unit was favored by rendering large π-delocalization attributed to the existence of the DEP[5]A macrocycle that occupies the cavity of the **DPAC-M** macrocycle.

In addition to the absorption spectra of macrocycle **DPAC-M** and [2]catenane **DPAC-C** that are slightly different from that of DPAC, their emission spectra are also different. For macrocycle **DPAC-M**, although the emission peaks at 550–700 nm are similar to that of DPAC, it can be clearly observed that the emission of macrocycle **DPAC-M** at 420–525 nm was greater than that of DPAC. These results indicate that even though the length of the alkyl chain linker in the macrocycle is long enough, the macrocyclic structure still to some extent affects the transition of the excited state of the DPAC unit from a bent conformation to a planar one. More importantly, in the case of

[2]catenane **DPAC-C**, the maximum emission peak revealed a significant blue shift to 580 nm. In addition, emission peaks at ~490 nm and ~625 nm were observed, indicating an interesting multiple emission property, which suggested that compared to the macrocyclic structure, the [2]catenane structure further affects the excited state transition of the inserted DPAC unit.

Subsequently, the effect of solvent viscosity on the VIE behaviors of macrocycle **DPAC-M** and [2]catenane **DPAC-C** was investigated. To highlight the key effects of the formation of macrocycle and [2]catenane on the precisely tunable emissions of the VIE system when changing solvent viscosity, the absorption and emission spectra of the DPAC unit at different EG ratios were first collected and the spectra indicated that the increase in EG ratio did not have a significant effect on the steady-state photophysical properties of the DPAC unit (Fig. S25a and S26†), while for macrocycle **DPAC-M**, as shown in Fig. 4c, the emission peak at 490 nm attributed to blue light emission enhanced with the increase of EG ratio. However, the fluorescence quantum yields ($\Phi_F$) did not show significant regular changes, ranging from 7.1% to 12.4% (Table S1†). These results demonstrated that for **DPAC-M** the intensity of short wavelength emission gradually enhanced with the increase of solvent viscosity, thus significantly strengthening the continuous configuration limitation of the DPAC unit in the excited state. In the case of [2]catenane **DPAC-C**, compared to macrocycle **DPAC-M**, the continuous configuration of the DPAC unit in the excited state is more significantly restricted upon increasing solvent viscosity, as revealed by the blue light emission when the proportion of EG reached 90% (Fig. 4d). Notably, a remarkable increase in the fluorescence quantum yields from 18.6% to 32.0% was also observed (Table S1†). As the viscosity of the solvent increases, the solutions of the macrocycle and [2]catenane also show significant colour changes at the macroscopic level: for macrocycle **DPAC-M**, the emission colour
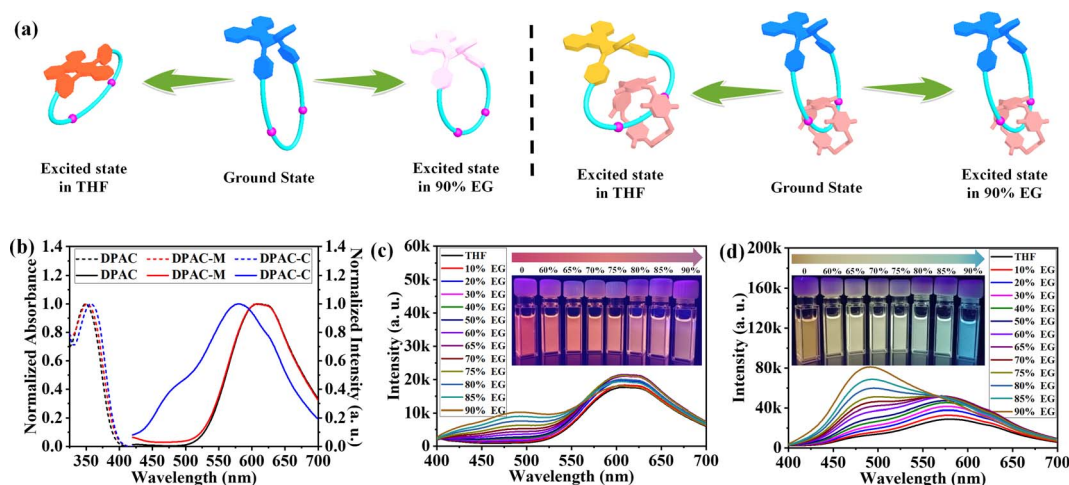


Fig. 4 (a) Cartoon representation of the ground and excited states of macrocycle **DPAC-M** and [2]catenane **DPAC-C**; (b) normalized absorption (dashed line) and fluorescence spectra (solid line) of DPAC, macrocycle **DPAC-M**, and [2]catenane **DPAC-C** in THF ($\lambda_{ex}$ = 360 nm, 0.01 mM); fluorescence spectra of macrocycle **DPAC-M** (c) and [2]catenane **DPAC-C** (d) in THF/EG with different EG fractions ($\lambda_{ex}$ = 360 nm, 0.01 mM). (Inset): Photographs upon UV lamp excitation at 365 nm.

gradually changes from orange red to pink (Fig. 4c: Inset), while for [2]catenane **DPAC-C**, the emission colour changes from yellow to light yellow, then to cyan, and finally to blue (Fig. 4d: Inset). The 1931 CIE coordinate diagram corresponding to different solvent viscosities clearly shows these colour transformation processes (Fig. S27 and Table S2†).

### Femtosecond transient absorption (TA) spectra of the VIE-active macrocycle and [2]catenane

To gain a better understanding of such interesting tunable VIE behaviors of the DPAC-functionalized macrocycle and [2]catenane, femtosecond transient absorption (TA) spectroscopy was performed under 360 nm excitation. Since the TA tests require high concentration, the steady-state photophysical properties of macrocycle **DPAC-M** and [2]catenane **DPAC-C** at a higher concentration (0.05 mM) were first measured before the TA tests (Fig. S28 and S29†). For macrocycle **DPAC-M**, compared with that in lower concentration (0.01 mM), only an increase in absorption and emission intensity was observed at different solvent viscosities (Fig. S28a and S29a†), while the CIE coordinates were similar (Fig. S30a and Table S3†), indicating that the concentration did not significantly affect the molecular vibrational relaxation process. However, in the case of [2]catenane **DPAC-C**, when the proportion of EG reached 90%, [2]catenane **DPAC-C** started to aggregate and precipitate (Fig. S28b and S29b†), which might hamper the further investigations of excited-state dynamics. Thus, the maximum proportion of EG

was set at 85% when investigating the solvent viscosity effect on the excited state conformations of the DPAC unit in [2]catenane **DPAC-C**.

As revealed by the TA spectra of macrocycle **DPAC-M** and [2]catenane **DPAC-C** in THF (Fig. 5b, d, S31 and S33†), compared to that of the sole DPAC unit,[23] their initial excited-state absorption (ESA) wavelengths were identical, and thus we speculated that the excited-state dynamics of both the macrocycle and [2]catenane in THF also include the whole process $R^* \rightarrow I_1^* \rightarrow I_2^* \rightarrow P^*$ (Fig. 5a). Therefore, on the basis of previous reports and with the aid of the GloTarAn program,[24] we performed the global analysis with a sequential five-component model on these TA data (Fig. 5b and d). Notably, by comparing stimulated emission (SE) in TA and the steady state fluorescence spectra, it can be proven that these species are emissive due to their corresponding relationship. For example, for the TA spectrum of macrocycle **DPAC-M** in THF (Fig. 5b), significant SE in the ranges of 400–480 nm (the second species, red line), 440–560 nm (the third species, green line), and 520–660 nm (the fourth species, blue line) was observed in the evolution associated difference spectra (EADS) obtained through the global analysis, which corresponds to weak emissions in the range of 400–525 nm and strong emissions in the range of 600–625 nm (Fig. S29a†).

According to the five-component model on the TA data, four spectral species with lifetimes of 1.3 ps, 13 ps, 74 ps, and 7.5 ns, and a long-lived component for macrocycle **DPAC-M**, and 2.4 ps, 30 ps, 390 ps, and 7.4 ns, and a long-lived component for [2]
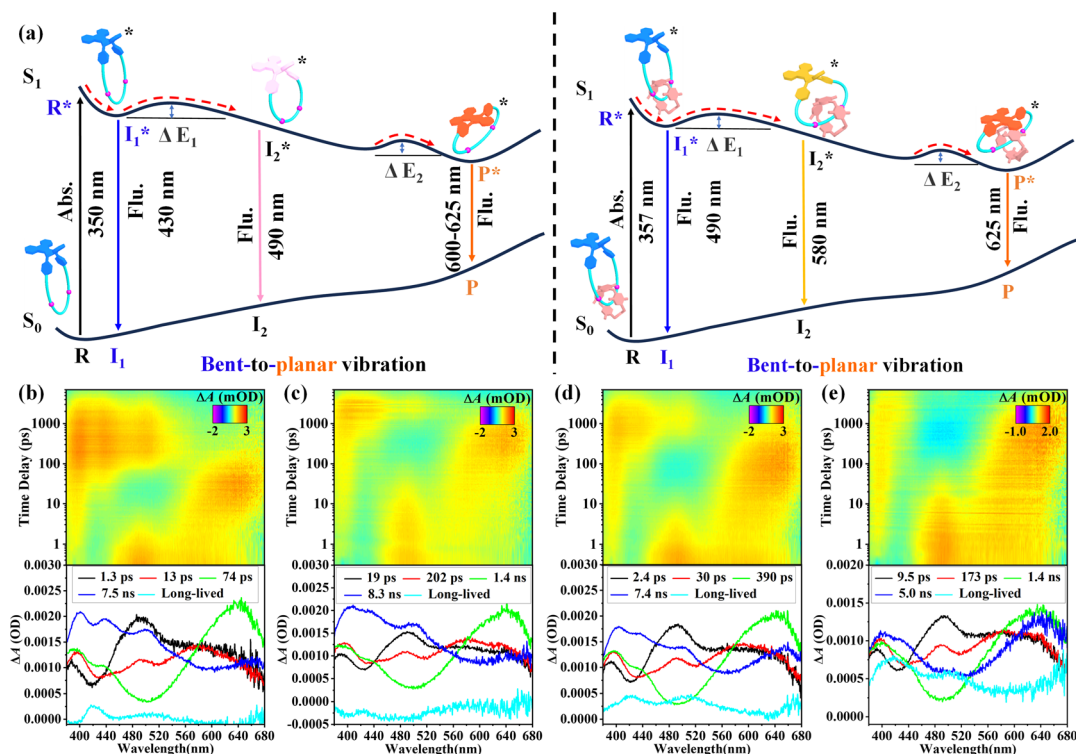


Fig. 5 (a) Schematic potential energy surfaces for the conformational evolution of macrocycle **DPAC-M** and [2]catenane **DPAC-C**; femtosecond transient absorption spectra of macrocycle **DPAC-M** in THF (b) and in THF/EG (v/v = 10/90) (c), and [2]catenane **DPAC-C** in THF (d) and in THF/EG (v/v = 15/85) (e) with a photoexcitation of 360 nm and corresponding evolution associated difference spectra (EADS) obtained through global analysis.

**Table 1** Lifetimes obtained from global analysis of transient absorption spectra

| Lifetimes | $\tau_1$/ps ($R^*$) | $\tau_2$/ps ($I_1^*$) | $\tau_3$ ($I_2^*$) | $\tau_4$/ns ($P^*$) | $\tau_5$ (long-lived) |
|---|---|---|---|---|---|
| **DPAC-M** in THF | $1.3 \pm 0.1$ | $13 \pm 0.3$ | $74 \pm 0.9$ ps | $7.5 \pm 0.3$ | — |
| **DPAC-C** in THF | $2.4 \pm 0.1$ | $30 \pm 0.5$ | $390 \pm 5.9$ ps | $7.4 \pm 0.3$ | — |
| **DPAC-M** in THF/EG (v/v = 10/90) | $19 \pm 0.8$ | $202 \pm 5.9$ | $1.4 \pm 0.1$ ns | $8.3 \pm 0.5$ | — |
| **DPAC-C** in THF/EG (v/v = 15/85) | $9.5 \pm 0.5$ | $173 \pm 5.2$ | $1.4 \pm 0.1$ ns | $5.0 \pm 0.2$ | — |

catenane **DPAC-C** were obtained (Table 1). For macrocycle **DPAC-M**, compared to the lifetimes of DPAC ($R^*$, 1.0 ps; $I_1^*$, 3.7 ps; $I_2^*$, 10 ps; $P^*$, 5.0 ns), the significant increase in the lifetimes of $I_1^*$ and $I_2^*$ indicated that the transition energy barriers $\Delta E_1$ and $\Delta E_2$ of $I_1^* \rightarrow I_2^*$ and $I_2^* \rightarrow P^*$ in the macrocycle system significantly enhanced, ultimately leading to not only bright $P$ emission consistent with that of the sole DPAC unit, but also small $I_1$ and $I_2$ emissions in the range of 400–525 nm (Fig. 4c and S29a†). These results strongly demonstrated that the locking of the DPAC unit by an alkyl chain linker through the formation of the macrocycle can effectively regulate the excited state conformations of DPAC, while in the case of [2]catenane **DPAC-C**, the even longer lifetimes of $I_1^*$ and $I_2^*$ indicated relatively slower transitions from $I_1^*$ to $I_2^*$ and $I_2^*$ to $P^*$ compared with DPAC and macrocycle **DPAC-M**. Thus, the excited state population can be trapped at $I_1^*$ and $I_2^*$ states as well as the $P^*$ state, resulting in the ultra-broad triple band yellow fluorescence emission (Fig. 4d and S29b†). According to these results, the formation of the mechanical bond revealed a more significant effect on the regulation of the excited state conformations of DPAC.

Subsequently, the effect of solvent viscosity on the excited-state conformations of the DPAC unit in macrocycle **DPAC-M** and [2]catenane **DPAC-C** was investigated (Fig. 5c, e, S32 and S34†). For macrocycle **DPAC-M** (Fig. 5c and Table 1), when the EG proportion was set at 90%, it can be observed that the lifetimes of $I_1^*$ and $I_2^*$ were astonishingly different. In particular, the lifetime of $I_2^*$ reached the nanosecond level. Such significant enhancement in lifespan indicated that in a highly viscous solvent system, the transition energy barriers $\Delta E_1$ and $\Delta E_2$ of $I_1^* \rightarrow I_2^*$ and $I_2^* \rightarrow P^*$ significantly increased. Thus, multiple excited states could be stabilized, ultimately leading to a pink emission (Fig. 4c and S29a†). In the case of [2]catenane **DPAC-C** (Fig. 5f and Table 1), upon setting the EG proportion at 85%, longer lifetimes of $I_1^*$ and $I_2^*$ were also observed, again confirming that the high viscosity solvent system significantly enhances these transition energy barriers. More importantly, due to the presence of the mechanical bond, the existence of multiple excited states in [2]catenane led to a cyan emission (Fig. 4d and S29b†). It can be inferred that for [2]catenane, further increasing the viscosity of the solvent system will further limit the vibrational relaxation of the lowest excited state V-shaped bent conformation to the nearly planar structure, ultimately achieving blue emission of [2]catenane **DPAC-C**. Notably, to probe the surface crossing and population of a triplet state, the microsecond transient absorption spectra of **DPAC-M** and **DPAC-C** in THF and viscous solvents were

obtained. According to the results shown in Fig. S35,† their kinetics lifetimes in air and $N_2$ are the same, indicating that there is no surface crossing and population of a triplet state in **DPAC-M** and **DPAC-C**.

## Chiral resolution and circularly polarized luminescence performances of DPAC-functionalized [2]catenane

As confirmed above, the [2]catenane **DPAC-C** displays attractive tunable emission behaviors attributed to the further regulation of the VIE behavior of the **DPAC-M** macrocycle through catenation. Moreover, considering that the other macrocyclic component DEP[5]A reveals unique planar chirality, the integrated [2]catenane would display promising CPL performance. Thus, chiral stationary phase-high performance liquid chromatography (HPLC, IC column, mobile phase: ethyl acetate/*n*-hexane = 30 : 70) was used to resolve the [2]catenane **DPAC-C** (Fig. 6a). The area ratio of the two fractions was found to be 27.6 : 27.5, indicating the existence of a pair of stereoisomers of [2]catenane **DPAC-C** (Fig. 6b and S36–S38†). Each fraction was isolated using a semi-preparative chiral HPLC column, and both the enantiomeric e.e. values were measured to be greater than 99%, indicating the successful separation of [2]catenane enantiomers.

Furthermore, circular dichroism (CD) spectra of these two fractions were then measured, in which mirror-imaged peaks with the same intensity were observed, confirming the existence of enantiomers (Fig. 6c). More importantly, according to the CD spectra, particularly characteristic bands at 250 nm and 310 nm, the absolute configurations of chiral [2]catenanes in the first and second fractions were designated as *pS* with the DEP[5]A wheel in (*pS*, *pS*, *pS*, *pS*, *pS*) conformation and *pR* with the DEP[5]A wheel in (*pR*, *pR*, *pR*, *pR*, *pR*) conformation, respectively. It is worth noting that in the CD spectra, in addition to the peaks attributed to the chiral DEP[5]A wheel, the characteristic absorption peaks ascribed to the DPAC unit were also observed in the 330–400 nm range, indicating the chirality information transfer from DEP[5]A to DPAC in the ground state (Fig. 6c).

It is worth noting that the unique VIE behavior of DPAC provides the possibility for multi-color CPL switching based on chiral [2]catenanes *pS*/*pR*-**DPAC-C**. Unfortunately, although significant color changes were observed after changing the solvent viscosity, no CPL signal was detected (Fig. S39†), which may be due to the lack of efficient chirality information transfer in the excited state in the solution state. Thus, the CPL performances of these chiral [2]catenanes in cast films were then measured. Upon excitation with UV light ($\lambda_{ex}$ = 340 nm), both of
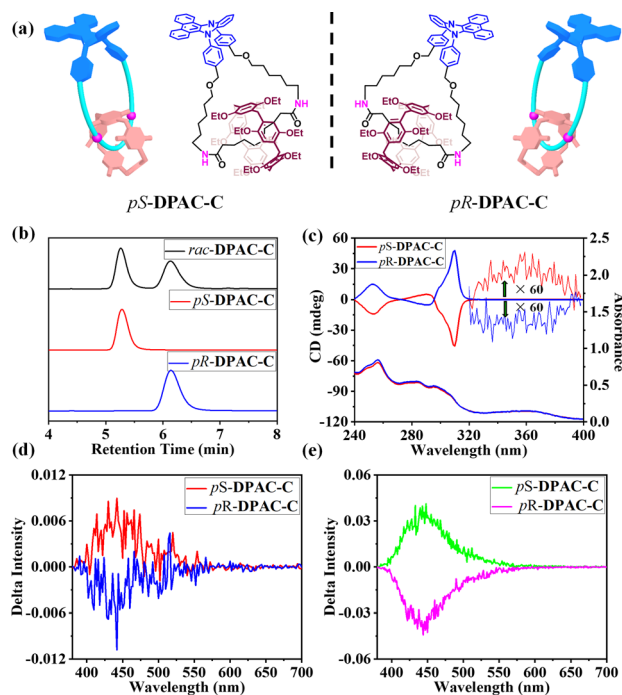
**Fig. 6** (a) Cartoon representation and chemical structures of a pair of enantiomers of **DPAC-C**; (b) chiral HPLC traces (ethyl acetate: *n*-hexane = 30 : 70, v/v); (c) solution-state ECD spectra and UV/vis absorption spectra (50 μM in THF) of chiral [2]catenanes *pS/pR*-**DPAC-C**; delta intensity of chiral [2]catenanes *pS/pR*-**DPAC-C** in cast films (d) and in KBr pellets (e).

these chiral [2]catenanes displayed strong CPL emissions at 450 nm that were attributed to the DPAC unit (Fig. 6d, S40a and c†), suggesting an efficient chirality information transmission in the excited state. As expected, the *pS/pR*-**DPAC-C** enantiomers revealed almost mirror-imaged CPL peaks with opposite $g_{lum}$, *i.e.*, a positive CPL signal for *pS*-**DPAC-C** with a $g_{lum}$ value of 2.46 $\times 10^{-3}$ and a negative CPL signal for *pR*-**DPAC-C** with a $g_{lum}$ value of $-2.68 \times 10^{-3}$, suggesting a pure CPL response. Interestingly, when dispersing these chiral [2]catenanes in the KBr pellet for testing (Fig. 6e, S40b and d†), even higher $g_{lum}$ values were observed (*pS*-**DPAC-C**, 4.79 $\times 10^{-3}$; *pR*-**DPAC-C**, $-5.08 \times 10^{-3}$), which might be attributed to the more orderly arrangements of chiral [2]catenanes in such media. Such impressive CPL performances, together with their tunable VIE behaviors, make these chiral [2]catenanes promising platforms for practical applications.

## Conclusions

In summary, aiming at investigating the effects of macrocyclization and catenation on the regulation of VIE behaviors, the typical VIE luminogen DPAC was introduced into a macrocycle and corresponding [2]catenane. By evaluating the VIE behaviors of the resultant DPAC-functionalized macrocycle and [2]catenane in detail with femtosecond transient absorption spectra, the crucial role of macrocyclization and catenation in capturing and stabilizing multiple excited states has been confirmed. In addition, the existence of the DEP[5]A macrocycle

with unique planar chirality as the other macrocyclic component endows the DPAC-functionalized [2]catenane with attractive CPL performances, making it the first CPL system based on VIE-active [2]catenane. According to our proof-of-concept study, the mechanical bond shows its great power for the development of novel molecular systems with tunable emission behaviors, thus further enabling the construction of promising platforms for the creation of novel smart chiral luminescent materials.

## Data availability

The authors declare that the data supporting the findings of this study are available within the paper and its ESI files.† All relevant data are available from the corresponding author on request.

## Author contributions

W. Wang, H.-B. Yang and X.-Q. Wang conceived the project; W.-T. Xu designed and performed the synthetic experiments, VIE and CPL studies with the help of Z. Peng, W.-J. Li and Y. Jiang; P. Wu and J. Chen designed and performed the TA studies; W. Wang, W.-T. Xu and H.-B. Yang prepared the manuscript.

## Conflicts of interest

There are no conflicts to declare.

## References

1 (*a*) J. Dai, H. Xue, D. Chen, X. Lou, F. Xia and S. Wang, *Coord. Chem. Rev.*, 2022, **464**, 214552; (*b*) J. Wu, J. Lin and P. Huang, *Chem. Soc. Rev.*, 2023, **52**, 3973–3990; (*c*) Y. Huang, L. Ning, X. Zhang, Q. Zhou, Q. Gong and Q. Zhang, *Chem. Soc. Rev.*, 2024, **53**, 1090–1166.

2 (*a*) X. Liu, D. Huang, C. Lai, G. Zeng, L. Qin, H. Wang, H. Yi, B. Li, S. Liu, M. Zhang, R. Deng, Y. Fu, L. Li, W. Xue and S. Chen, *Chem. Soc. Rev.*, 2019, **48**, 5266–5302; (*b*) J.-T. Hou, N. Kwon, S. Wang, B. Wang, X. He, J. Yoon and J. Shen, *Coord. Chem. Rev.*, 2022, **450**, 214232; (*c*) J. Ouyang, L. Sun, F. Zeng and S. Wu, *Coord. Chem. Rev.*, 2022, **458**, 214438; (*d*) Z. Wang, Y. Zhou, R. Xu, Y. Xu, D. Dang, Q. Shen, L. Meng and B. Z. Tang, *Coord. Chem. Rev.*, 2022, **451**, 214279.

3 (a) O. Ostroverkhova, *Chem. Rev.*, 2016, **116**, 13279–13412; (b) X. Ai, E. W. Evans, S. Dong, A. J. Gillett, H. Guo, Y. Chen, T. J. H. Hele, R. H. Friend and F. Li, *Nature*, 2018, **563**, 536–540; (c) X. Tang, L.-S. Cui, H.-C. Li, A. J. Gillett, F. Auras, Y.-K. Qu, C. Zhong, S. T. E. Jones, Z.-Q. Jiang, R. H. Friend and L.-S. Liao, *Nat. Mater.*, 2020, **19**, 1332–1338; (d) R. Gao, M. S. Kodaimati and D. Yan, *Chem. Soc. Rev.*, 2021, **50**, 5564–5589; (e) X.-Y. Lou, S. Zhang, Y. Wang and Y.-W. Yang, *Chem. Soc. Rev.*, 2023, **52**, 6644–6663.

4 (a) Z. Zhang, W. Wang, M. O'Hagan, J. Dai, J. Zhang and H. Tian, *Angew. Chem., Int. Ed.*, 2022, **61**, e202205758; (b) Y.-J. Ma, X. Fang, G. Xiao and D. Yan, *Angew. Chem., Int. Ed.*, 2022, **61**, e202114100.

5 C. Liu, K. Fu, S. Zheng, L. Yao, W. Zhou and G. Liu, *Adv. Opt. Mater.*, 2023, **11**, 2300019.

6 C. Ma, W. Sun, L. Xu, Y. Qian, J. Dai, G. Zhong, Y. Hou, J. Liu and B. Shen, *J. Mater. Chem. B*, 2020, **8**, 9642–9651.

7 Q. Zhang, L. Yang, Y. Han, Z. Wang, H. Li, S. Sun and Y. Xu, *Chem. Eng. J.*, 2022, **428**, 130986.

8 C. Shang, G. Wang, K. Liu, Q. Jiang, F. Liu, P.-T. Chou and Y. Fang, *Angew. Chem., Int. Ed.*, 2020, **59**, 8579–8585.

9 (a) Z. Fu, K. Wang and B. Zou, *Chin. Chem. Lett.*, 2019, **30**, 1883–1894; (b) C. Wang, Y. Yu, Y. Yuan, C. Ren, Q. Liao, J. Wang, Z. Chai, Q. Li and Z. Li, *Matter*, 2020, **2**, 181–193.

10 (a) D. Tu, P. Leong, S. Guo, H. Yan, C. Lu and Q. Zhao, *Angew. Chem., Int. Ed.*, 2017, **56**, 11370–11374; (b) K. Tabata, T. Yamada, H. Kita and Y. Yamamoto, *Adv. Funct. Mater.*, 2019, **29**, 1805824; (c) Z. Zhang, Y.-A. Chen, W.-Y. Hung, W.-F. Tang, Y.-H. Hsu, C.-L. Chen, F.-Y. Meng and P.-T. Chou, *Chem. Mater.*, 2016, **28**, 8815–8824; (d) J. X. Ong, C. S. Q. Lim, H. V. Le and W. H. Ang, *Angew. Chem., Int. Ed.*, 2019, **58**, 164–167; (e) A. C. Sedgwick, W.-T. Dou, J.-B. Jiao, L. Wu, G. T. Williams, A. T. A. Jenkins, S. D. Bull, J. L. Sessler, X.-P. He and T. D. James, *J. Am. Chem. Soc.*, 2018, **140**, 14267–14271; (f) J. Zhang, P. Alam, S. Zhang, H. Shen, L. Hu, H. H. Y. Sung, I. D. Williams, J. Sun, J. W. Y. Lam, H. Zhang and B. Z. Tang, *Nat. Commun.*, 2022, **13**, 3492.

11 (a) Z. Zhang, Y.-S. Wu, K.-C. Tang, C.-L. Chen, J.-W. Ho, J. Su, H. Tian and P.-T. Chou, *J. Am. Chem. Soc.*, 2015, **137**, 8509–8520; (b) W. Huang, L. Sun, Z. Zheng, J. Su and H. Tian, *Chem. Commun.*, 2015, **51**, 4462–4464; (c) Z. Zhang, G. Sun, W. Chen, J. Su and H. Tian, *Chem. Sci.*, 2020, **11**, 7525–7537; (d) Z. Zhang, W. Song, J. Su and H. Tian, *Adv. Funct. Mater.*, 2020, **30**, 1902803; (e) Z. Zhang, X. Jin, X. Sun, J. Su and D.-H. Qu, *Coord. Chem. Rev.*, 2022, **472**, 214768; (f) S. Qiu, Z. Zhang, Z. Wang, D.-H. Qu and H. Tian, *Precis. Chem.*, 2023, **1**, 129–138; (g) S. Qiu, Z. Zhang, Y. Wu, F. Tong, K. Chen, G. Liu, L. Zhang, Z. Wang, D.-H. Qu and H. Tian, *CCS Chem.*, 2022, **4**, 2344–2353.

12 (a) H. Zhou, J. Mei, Y.-A. Chen, C.-L. Chen, W. Chen, Z. Zhang, J. Su, P.-T. Chou and H. Tian, *Small*, 2016, **12**, 6542–6546; (b) W. Chen, C. Guo, Q. He, X. Chi, V. M. Lynch, Z. Zhang, J. Su, H. Tian and J. L. Sessler, *J. Am. Chem. Soc.*, 2019, **141**, 14798–14806; (c) Z. Zong, Q. Zhang and D.-H. Qu, *CCS Chem.*, 2024, **6**, 774–782.

13 (a) L. Shi, W. Song, C. Lian, W. Chen, J. Mei, J. Su, H. Liu and H. Tian, *Adv. Opt. Mater.*, 2018, **6**, 1800190; (b) Y. Zhang, Y. Li, H. Wang, Z. Zhang, Y. Feng, Q. Tian, N. Li, J. Mei, J. Su and H. Tian, *ACS Appl. Mater. Interfaces*, 2019, **11**, 39351–39358; (c) W. Song, W. Ye, L. Shi, J. Huang, Z. Zhang, J. Mei, J. Su and H. Tian, *Mater. Horiz.*, 2020, **7**, 615–623; (d) Y. Su, H. Liu, X. Chen, Q. Wang, J. Su and Z. Zhang, *ACS Appl. Polym. Mater.*, 2022, **4**, 1636–1642; (e) F. Gu, Y. Li, T. Jiang, J. Su and X. Ma, *CCS Chem.*, 2022, **4**, 3014–3022.

14 (a) Q. Gong, W. Qin, P. Xiao, X. Wu, L. Li, G. Zhang, R. Zhang, J. Sun, S. Q. Yao and W. Huang, *Chem. Commun.*, 2020, **56**, 58–61; (b) J. Ramos-Soriano, S. J. Benitez-Benitez, A. P. Davis and M. C. Galan, *Angew. Chem., Int. Ed.*, 2021, **60**, 16880–16884; (c) W.-T. Dou, X. Wang, T. Liu, S. Zhao, J.-J. Liu, Y. Yan, J. Li, C.-Y. Zhang, A. C. Sedgwick, H. Tian, J. L. Sessler, D.-M. Zhou and X.-P. He, *Chem*, 2022, **8**, 1750–1761.

15 (a) J. Wang, X. Yao, Y. Liu, H. Zhou, W. Chen, G. Sun, J. Su, X. Ma and H. Tian, *Adv. Opt. Mater.*, 2018, **6**, 1800074; (b) G. Sun, J. Pan, Y. Wu, Y. Liu, W. Chen, Z. Zhang and J. Su, *ACS Appl. Mater. Interfaces*, 2020, **12**, 10875–10882; (c) S. Liu, J. Wang, F. Tang, N. Wang, L. Li, C. Yao and L. Li, *ACS Appl. Mater. Interfaces*, 2020, **12**, 55269–55277; (d) X. Chen, J. Chen, G. Sun, L. Guo, J. Su and Z. Zhang, *ACS Appl. Mater. Interfaces*, 2021, **13**, 38629–38636; (e) Y. Hu, Z. Huang, I. Willner and X. Ma, *CCS Chem.*, 2024, **6**, 518–527.

16 (a) Z. Zong, Q. Zhang, S.-H. Qiu, Q. Wang, C. Zhao, C.-X. Zhao, H. Tian and D.-H. Qu, *Angew. Chem., Int. Ed.*, 2022, **61**, e202116414; (b) Z. Zhou, D.-G. Chen, M. L. Saha, H. Wang, X. Li, P.-T. Chou and P. J. Stang, *J. Am. Chem. Soc.*, 2019, **141**, 5535–5543; (c) W. Chen, C.-L. Chen, Z. Zhang, Y.-A. Chen, W.-C. Chao, J. Su, H. Tian and P.-T. Chou, *J. Am. Chem. Soc.*, 2017, **139**, 1636–1644; (d) S. Qiu, Y. Zhao, L. Zhang, Y. Ni, Y. Wu, H. Cong, D.-H. Qu, W. Jiang, J. Wu, H. Tian and Z. Wang, *CCS Chem.*, 2023, **5**, 1763–1772.

17 (a) J. F. Stoddart, *Chem. Soc. Rev.*, 2009, **38**, 1802; (b) R. S. Forgan, J. P. Sauvage and J. F. Stoddart, *Chem. Rev.*, 2011, **111**, 5434–5464; (c) E. A. Neal and S. M. Goldup, *Chem. Commun.*, 2014, **50**, 5128–5142; (d) C. J. Bruns and J. F. Stoddart, *The Nature of the Mechanical Bond: From Molecules to Machines*, John Wiley and Sons, Hoboken, 2016; (e) J. E. M. Lewis, M. Galli and S. M. Goldup, *Chem. Commun.*, 2017, **53**, 298–312; (f) M. Denis and S. M. Goldup, *Nat. Rev. Chem*, 2017, **1**, 0061; (g) H. Y. Zhou, Y. Han and C. F. Chen, *Mater. Chem. Front.*, 2020, **4**, 12–28; (h) D. Sluysmans and J. F. Stoddart, *Trends Chem.*, 2019, **1**, 185; (i) J.-X. Liu, K. Chen and C. Redshaw, *Chem. Soc. Rev.*, 2023, **52**, 1428–1455; (j) A. H. G. David and J. F. Stoddart, *Isr. J. Chem.*, 2021, **61**, 608–621.

18 (a) S. Yang, C.-X. Zhao, S. Crespi, X. Li, Q. Zhang, Z.-Y. Zhang, J. Mei, H. Tian and D.-H. Qu, *Chem*, 2021, **7**, 1544–1556; (b) C. Yu, X. Wang, C.-X. Zhao, S. Yang, J. Gan, Z. Wang, Z. Cao and D.-H. Qu, *Chin. Chem. Lett.*, 2022, **33**, 4904–4907; (c) P. Rajamalli, F. Rizzi, W. Li, M. A. Jinks, A. K. Gupta, B. A. Laidlaw, I. D. W. Samuel, T. J. Penfold,

S. M. Goldup and E. Zysman-Colman, *Angew. Chem., Int. Ed.*, 2021, **60**, 12066–12073.

19 (*a*) W. Wang, L.-J. Chen, X.-Q. Wang, B. Sun, X. Li, Y. Zhang, J. Shi, Y. Yu, L. Zhang, M. Liu and H.-B. Yang, *Proc. Natl. Acad. Sci. U. S. A.*, 2015, **112**, 5597–5601; (*b*) X.-Q. Wang, W. Wang, W.-J. Li, L.-J. Chen, R. Yao, G.-Q. Yin, Y.-X. Wang, Y. Zhang, J. Huang, H. Tan, Y. Yu, X. Li, L. Xu and H.-B. Yang, *Nat. Commun.*, 2018, **9**, 3190; (*c*) X.-Q. Wang, W.-J. Li, W. Wang, J. Wen, Y. Zhang, H. Tan and H.-B. Yang, *J. Am. Chem. Soc.*, 2019, **141**, 13923–13930; (*d*) W.-J. Li, Z. Hu, L. Xu, X.-Q. Wang, W. Wang, G.-Q. Yin, D.-Y. Zhang, Z. Sun, X. Li, H. Sun and H.-B. Yang, *J. Am. Chem. Soc.*, 2020, **142**, 16748–16756; (*e*) W.-J. Li, W. Wang, X.-Q. Wang, M. Li, Y. Ke, R. Yao, J. Wen, G.-Q. Yin, B. Jiang, X. Li, P. Yin and H.-B. Yang, *J. Am. Chem. Soc.*, 2020, **142**, 8473–8482; (*f*) W.-J. Li, X.-Q. Wang, D.-Y. Zhang, Y.-X. Hu, W.-T. Xu, L. Xu, W. Wang and H.-B. Yang, *Angew. Chem., Int. Ed.*, 2021, **60**, 18761–18768; (*g*) W.-J. Li, W.-T. Xu, X.-Q. Wang, Y. Jiang, Y. Zhu, D.-Y. Zhang, X.-Q. Xu, L.-R. Hu, W. Wang and H.-B. Yang, *J. Am. Chem. Soc.*, 2023, **145**, 14498–14509; (*h*) X.-Q. Wang, W.-J. Li, W. Wang and H.-B. Yang, *Acc. Chem. Res.*, 2021, **54**, 4091–4106; (*i*) Y. Zhu, H. Jiang, W. Wu, X.-Q. Xu, X.-Q. Wang, W.-J. Li, W.-T. Xu, G. Liu, Y. Ke, W. Wang and H.-B. Yang, *Nat. Commun.*, 2023, **14**, 5307; (*j*) D.-Y. Zhang, Y. Sang, T. K. Das, Z. Guan, N. Zhong, C.-G. Duan, W. Wang, J. Fransson, R. Naaman and H.-B. Yang, *J. Am. Chem. Soc.*, 2023, **145**, 26791–26798.

20 (*a*) W.-J. Li, Q. Gu, X.-Q. Wang, D.-Y. Zhang, Y.-T. Wang, X. He, W. Wang and H.-B. Yang, *Angew. Chem., Int. Ed.*, 2021, **60**, 9507–9515; (*b*) Y. Wang, J. Gong, X. Wang, W.-J. Li, X.-Q. Wang, X. He, W. Wang and H.-B. Yang, *Angew. Chem., Int. Ed.*, 2022, **61**, e202210542.

21 (*a*) S. Fa, T. Kakuta, T.-a. Yamagishi and T. Ogoshi, *Chem. Lett.*, 2019, **48**, 1278–1287; (*b*) J.-F. Chen, J.-D. Ding and T.-B. Wei, *Chem. Commun.*, 2021, **57**, 9029–9039; (*c*) C. Shi, H. Li, X. Shi, L. Zhao and H. Qiu, *Chin. Chem. Lett.*, 2022, **33**, 3613–3622; (*d*) T. Zhao, W. Wu and C. Yang, *Chem. Commun.*, 2023, **59**, 11469–11483; (*e*) K. Kato, S. Fa and T. Ogoshi, *Angew. Chem., Int. Ed.*, 2023, **62**, e202308316; (*f*) K. Kato, S. Fa, S. Ohtani, T.-h. Shi, A. M. Brouwer and T. Ogoshi, *Chem. Soc. Rev.*, 2022, **51**, 3648–3687.

22 (*a*) I. Nierengarten, E. Meichsner, M. Holler, P. Pieper, R. Deschenaux, B. Delavaux-Nicot and J.-F. Nierengarten, *Chem.–Eur. J.*, 2018, **24**, 169–177; (*b*) M. Rémy, I. Nierengarten, B. Park, M. Holler, U. Hahn and J.-F. Nierengarten, *Chem.–Eur. J.*, 2021, **27**, 8492–8499; (*c*) N. Becharguia, E. Wasielewski, R. Abidi, I. Nierengarten and J.-F. Nierengarten, *Chem.–Eur. J.*, 2024, **30**, e202303501; (*d*) N. Becharguia, I. Nierengarten, J.-M. Strub, S. Cianférani, M. Rémy, E. Wasielewski, R. Abidi and J.-F. Nierengarten, *Chem.–Eur. J.*, 2024, e202304131; (*e*) Z. Peng, P.-P. Jia, X.-Q. Wang, X.-L. Zhao, H.-B. Yang and W. Wang, *CCS Chem.*, 2024, DOI: **10.31635/ccschem.024.202303738**.

23 (*a*) W.-T. Xu, X. Li, P. Wu, W.-J. Li, Y. Wang, X.-Q. Xu, X.-Q. Wang, J. Chen, H.-B. Yang and W. Wang, *Angew. Chem., Int. Ed.*, 2024, **63**, e202319502; (*b*) X. Jin, S. Guo, X. Wang, M. Cong, J. Chen, Z. Zhang, J. Su, D.-H. Qu and H. Tian, *Angew. Chem., Int. Ed.*, 2023, **62**, e202305572.

24 J. J. Snellenburg, S. P. Laptenok, R. Seger, K. M. Mullen and I. H. M. van Stokkum, *J. Stat. Software*, 2012, **49**, 1–22.